***Application of AC-SECM in Corrosion Science - Local Visualisation of Inhibitor Films on Active Metals for Corrosion Protection***

Maike Pähler[a], Juan José Santana[b], Wolfgang Schuhmann[a], Ricardo M. Souto[b]

[a]*Analytische Chemie - Elektroanalytik & Sensorik; Ruhr-Universität Bochum, Universitätsstraße 150, D-44780 Bochum, Germany*

[b]*Department of Physical Chemistry, University of La Laguna, E-38200 La Laguna, Tenerife, Canary Islands, Spain*

**Abstract**

The suitability of frequency-dependent alternating-current scanning electrochemical microscopy (4D AC-SECM) for the investigation of the thin passivating layers covering the surface of corrosion-inhibited metals has been demonstrated. The inhibition of copper corrosion by benzotriazole (BTAH) and methyl-benzotriazole (MBTAH), which are effective inhibitors for this metal in many environmental conditions, was investigated. Strong dependencies were found for the AC *z*-approach curves with both the duration of the inhibitor treatment and the frequency of the AC excitation signal applied in AC-SECM. Both negative and positive feedback behaviours were observed in the AC approach curves for untreated copper and for Cu-BTAH and Cu-MBTAH samples. Negative feedback behaviour occurred in the low frequency range, whereas the positive feedback effect was observed at higher frequencies. A threshold frequency related to the passage from negative to positive regimes could be determined in each case. The value of the threshold frequency for inhibitor-modified samples was found always to be significantly higher than for the untreated metal, because the inhibitor film provides electrical insulation for the surface. Moreover, the threshold frequency increased with greater surface coverage by the inhibitor. 3D AC-SECM was successfully applied to visualizing spatially-resolved differences in the local electrochemical activity between inhibitor-free and inhibitor-covered areas of the sample.

## Introduction

The major part of the current knowledge of corrosion processes has been gained from the use of conventional electrochemical methods such as cyclic voltammetry, chronoamperometry and electrochemical impedance spectroscopy (EIS). Whatever the measurable quantity, it reflects the reactivity of the whole electrode surface; in other words, its analysis is based on the assumption that the electrochemical behaviour of the interface is uniform, and the monitored signal corresponds to an average measurement over the whole electrode surface. Unfortunately, the corrosion of most metals and alloys does not occur uniformly over the surface but they are originating from various forms of localized corrosion processes such as pitting corrosion, crack corrosion or intergranular corrosion among others. But all corrosion processes, either generalized or localized from a macroscopic standpoint, have in common that they are initiated within the range of nanometers and micrometers, and a comprehensive understanding of the mechanistic aspects of corrosion requires the acquisition of data obtained in those scales. Unfortunately, conventional electrochemical techniques lack spatial resolution and provide little information on the behaviour at sites of corrosion initiation or at defects.

Thus, there is need for techniques with enhanced spatial resolution which can acquire data in real time and can hence provide corroborative evidence of the underlying reaction schemes preferably *in situ*. In this way, microelectrochemical techniques are becoming essential tools in the study of corrosion processes. Among them, the scanning electrochemical microscope (SECM) has gained a fast growing interest within the corrosion science community due to its ability to provide *in situ* topographic and electrochemical reactivity information about the surface evolution at the micrometer and submicrometer scale in aqueous solution. In this way, this technique has proven to be a very useful tool for studying a wide range of corrosion processes covering bimetallic corrosion [1-3], the dissolution of inclusions in alloys [4-6], the controlled generation of single pits in otherwise passive metals [7-9], the monitoring of precursor sites for pit nucleation in oxide layers [10-12] and the detection of the metastable pitting regime [13,14], or the onset of corrosion processes from defective coatings [15-18]. A recent review on further uses of SECM in the field of corrosion can be found in ref. [19].

Despite the various detection schemes developed for scanning electrochemical microscopy operation such as the amperometric feedback mode [20], generator–collector mode [21] or redox competition mode [22] among others, the technique always involves the measurement of faradaic current at the microelectrode tip. Thus, the addition of a freely diffusing redox species to the electrolytic phase is often employed. This may represent a problem in many systems, as it may modify the electrical state of the investigated surface either by affecting its corresponding Nernst potential in the electrolyte, or even shifting chemical and electrochemical equilibria occurring at the substrate [23]. Indeed, the addition of a redox mediator is always required for the investigation of metallic systems covered by insulating films or layers such as those employed for corrosion

protection when they do not exhibit detectable flaws of continuity [24]. Such insulating films are found when the metal is coated with a polymeric film (i.e., anticorrosion paints and varnishes) resulting in the formation of inhibitor films due to the interaction of organic molecules with the metallic surface. These layers introduce a physical barrier between the underlying metal and the electrolytic environment, and greatly hinder the investigation of such highly resistive systems. This is reflected by the scarce number of publications concerning the characterization of intact polymer coatings on metals [25-27] or for corrosion protection with inhibitors [28-31], though both are topics of major interest in corrosion science. And even then, the eventual transport of the added redox mediator through the surface layers into the polymeric matrix and towards the metal-organic film interface cannot be discarded to occur, at least for sufficiently long exposure times, thus greatly limiting the applicability of the method. An additional requirement of conventional amperometric SECM is that sufficiently high conductive electrolytes are employed to exclude the participation of the diffusing redox species in migration or convective transport processes, though many real corrosion processes actually occur in poorly conductive environments.

A very interesting alternative for the study of highly resistive surfaces arises from the recent development of frequency-dependent alternating-current scanning electrochemical microscopy (4D AC-SECM) [32]. By applying an alternating potential to a microelectrode used as SECM-tip and recording the alternating current response spatially-resolved information on the electrochemical behaviour of heterogeneous samples becomes available [33]. The current magnitude as well as its phase shift with respect to the applied AC potential modulation are recorded, which carry information about local surface properties such as local conductivities and local ion concentrations. The near field interaction between the SECM tip and surface depends mainly on the solution resistance, the nature of the investigated surface [33-39] and on the applied perturbation frequency [32,33]. Therefore, it is consequent to perform frequency spectra at each point of the scanning grid to get multi-frequency AC-SECM images displaying the frequency-dependent AC current magnitude responses [39]. Therefore, conversely to what happens in conventional amperometric SECM, this technique is not based on the measurement of a redox process, thus avoiding the addition of a diffusing redox mediator, and it operates in highly diluted electrolytes. The applicability of 4D AC-SECM to the investigation of active corrosion processes has been successfully demonstrated to image corrosion pits in passivated steels and defects in polymer-coated metals [34,39-41], and to monitor the selective metal dissolution of alloys [42,43].

From the foregoing, we regard 4D AC-SECM to be a promising tool for the analysis of the thin surface layers produced for many inhibitor-metal systems. To demonstrate the feasibility of this approach, copper was chosen as a representative metal model because this is a base metal with a low redox potential in aqueous solutions, and copper oxi-hydroxide passivating films are readily formed in air as well as in neutral and alkaline aqueous environments. The chosen inhibitor system for copper corrosion for this investigation was either benzotriazole (BTAH) or methyl-benzotrizole

(MBTAH). These two organic molecules are widely employed as corrosion inhibitors for copper and its alloys [44, and references cited therein], and it is known that the protecting effect of BTAH is based on the formation of a polymeric $[Cu(I)BTAH]_n$ film on the surface of the electrode [45-47]. The only antecedents for such study by employing microelectrochemical scanning techniques are to be found in the SECM-based investigations of benzotriazole films using *z*-approach curves on polarized copper by Mansikkamäki et al. [28-30], and on non-polarized copper samples using both *z*-approach curves and 3D topographic maps of the surface by Izquierdo et al. [31]. In those studies, ferrocene-methanol had to be added to the test electrolyte to serve as freely diffusing redox mediator, though it might influence the corrosion process on the metal surface.

**Results and discussion**

Figure 1 shows a selection of the AC approach curves determined from a freshly-polished copper surface immersed in 1 mM $Na_2SO_4$ electrolyte in a frequency range of 351 to 55493 Hz. These plots have been normalized in both axis.

Two different trends for the variation of the current magnitude with the tip-to-sample distance were found for this system within the frequency range under consideration. In the first case, the current magnitude is progressively decreasing from its value in the bulk electrolyte as the tip moves towards the sample. This negative feedback type behaviour for the untreated copper sample in the test electrolyte applies to the low frequency AC approach curves measured at 966 and 3257 Hz. On the other hand, the opposite behaviour is observed for all the other AC approach curves depicted in figure 1. They exhibit greater current magnitudes compared to the bulk value at all distances and frequencies, their values continuously increasing as the tip continuously approaches the copper surface. The magnitude of this positive feedback type effect is observed to be dependent on the frequency of the AC signal, and it is highest at the high frequency limit. The AC approach curve determined at the frequency of 8966 Hz only exhibits a week positive feedback effect. Obviously, this frequency value is only slightly higher than the frequency at which the transition from negative to positive feedback type behaviour occurs.

The different feedback behaviour displayed by insulating and conducting surfaces in AC approach curves can also be applied to the characterization of the thin surface films formed during the adsorption of corrosion inhibitors on metals. These organic molecules will modify the original conductive characteristics typical of the bare metal into varying degrees of insulating character depending on the extent of surface coverage and the imparting barrier effects conferred to the metal-inhibitor system by these inhibiting layers [28,31]. In this way, the electrochemical activity and inhibiting properties of copper surfaces modified by triazoles can be investigated by 4D AC-SECM. The triazole compounds investigated were benzotriazole (BTAH) and 5-methyl-1H-benzotrizole (MBTAH).

A selection of the AC approach curves measured for Cu-BTAH samples immersed in 1 mM $Na_2SO_4$ in a frequency range from 351 to 55493 Hz and for various durations of sample pre-treatment in the inhibitor containing solution is given in figure 2. Direct comparison between the AC approach curves for the Cu-BTAH and the untreated copper samples demonstrates that the amplitude of the positive feedback type effect is significantly smaller for the BTAH-modified samples. Moreover, a positive feedback type behaviour is only found at the highest frequencies. The adsorption of the BTAH molecules on copper leads to the formation of a resistive film on the metal surface thus effectively protecting the metal against corrosion. The protective effect is considered to arise from the inhibitor-containing film on the metal and not from the copper oxide layer since the reported effect was also found with conventional SECM on polarized copper samples for varying oxygen concentrations in the electrolyte [29]. It must also be noticed that a perfectly insulating barrier film is not produced with the dipping procedure employed in this work even for the longest pre-treatment applied. A perfect insulating barrier would have resulted only in the measurement of negative feedback type AC approach curves even at the highest frequencies.

Furthermore, the threshold frequency at which the change from negative to positive feedback behaviour occurs is shifting to higher frequency values for the inhibited surfaces. For instance, the current magnitude of the approach curve measured at 8966 Hz in case of the Cu-BTAH samples always show negative feedback type behaviour whereas positive feedback was observed at this frequency for the untreated copper (cf. figure 1). The threshold frequencies for Cu-BTAH are close to 16242 Hz for the samples pre-treated during 5 minutes, and ca. 20158 Hz for the longer treatments.

Additional observations can be derived from a closer inspection of the AC approach curves for the Cu-BTAH system for different durations of the pre-treatment step in the inhibitor-containing solution. A very thin protecting layer should be expected for the samples treated for 5 min, whereas the system seems to be almost stationary after 30 min pre-treatment as concluded from the same threshold frequencies for the samples treated with the inhibitor for 30 and 60 min. Additionally, there is a decrease in the magnitude of the positive feedback type effect measured at the highest frequency for the samples treated for a longer period in the inhibitor-containing electrolyte. The normalized amplitude values at the closest proximity to the samples are 1.281 for the sample treated for 5 min, to 1.220 for the 30 min treatment, and 1.165 for the longest one. It may be considered that this decrease in the current magnitude at the highest frequency is related to the inhibiting efficiency of the system.

A similar behaviour was observed in the case of the Cu-MBTAH system from the inspection of the corresponding AC approach curves shown in figure 3. Both the frequency dependence and the magnitude of the positive and negative feedback type effects in the approach curves strongly vary among the samples as a result of the duration of their contact with the MBTAH-containing solution. Negative feedback type behaviour is always observed at the lowest frequency values and

it progressively changes until a positive feedback effect arises at the highest frequencies reached. The threshold frequency at which the negative to positive feedback crossing occurs moves towards higher frequency values as the copper samples were left in contact with the MBTAH solution for longer periods of time.

In order to explain the reported observations, an equivalent circuit can be employed as shown in figure 4 can be employed [39]. The dotted box in the figure gives the equivalent circuit that applies for a conductive surface exposed to a low conductivity environment. The equivalent circuit consists of the resistance and the capacitance of the tip, $R_T$ and $C_T$ respectively; and the solution resistance $R_{sol}$. Since $R_{sol}$ changes with the absolute *z* distance between the tip and the sample surface, this is the origin of the near-field response observed in the system. Thus, depending on the applied frequency and the electrochemical characteristics of the surface, the current will preferentially flow through one of the pathways depicted in the figure depending on their corresponding impedances. In this case, the capacitive impedance dominates over the solution impedance while it varies inversely with the frequency of the AC excitation. The negative feedback type effect is observed when the frequency of the signal is smaller than the reversal of the time constant for the interfacial impedance, whereas a positive feedback effect will be observed for frequencies equal or greater than that time constant. This is the rationale behind the observation of a threshold frequency for a conductive system such as that provided by the untreated copper metal in the test electrolyte, which corresponded to ca.8.9 Hz in our case.

When the copper samples are modified by the organic molecules acting as corrosion inhibitors, new components must be included into the equivalent circuit to account for the increased impedance introduced by the inhibitor film. The new components are: $R_S$ and $C_S$, the resistance and capacitance of the sample, respectively; and $R_{S'}$ and $C_{S'}$, and the local resistance and capacitance of the sample at the specific area covered by the AC-SECM tip, respectively. The impedance values derived from these additional components in the equivalent circuit will strongly depend on the duration of the pre-treatment process. In this way, the four parameters will change, and the corresponding time constants will also vary. When the tip approaches the inhibitor-modified copper surface, changes will occur in $C_{S'}$, which corresponds to the surface below the scanning tip, with the result that a different threshold frequency will be found for each system. Both for the Cu-BTAH and the Cu-MBTAH samples the threshold frequencies are observed to shift to higher values as the surface coverage of the metal surface by the inhibitor also increases, which can be explained by the insulating character of the inhibitor film.

Furthermore, changes in the slopes of the AC approach curves for varying frequencies and pre-treatment durations are observed for the Cu-BTAH and Cu-MBTAH systems. Longer pre-treatments lead to approach curves with smaller slopes at the highest frequencies resulting from the less conductive characteristics of the modified surfaces. Indeed, the normalized amplitude for the highest frequency value of 37.01 kHz can be regarded to be almost constant for normalized

distances below 0.2 for both the Cu-BTAH and the Cu-MBTAH systems when they were pre-treated in the inhibitor-containing electrolyte for 30 and 60 min. Conversely, an ever increasing positive feedback type effect is observed at that frequency for the samples pre-treated for 5 min. This may be regarded as an indication that full coverage of the metal surface was not achieved during shorter treatments. On the other hand, the adsorption of BTAH on copper is slower than that of MBTAH from the observation of lower threshold frequencies for benzotriazole that for the methyl-substituted molecule for a given duration of the pre-treatment step.

Surface imaging can also be performed by AC-SECM. In this case, a frequency spectra was applied at each point of the scanning grid and after the scan was completed, the image with the best contrast was chosen. From the comparison of the plots depicted in figures 1-3, the frequency value 8.966 kHz was chosen to provide the best contrast between the Cu-inhibitor and the bare Cu surfaces. The AC-SECM image of a copper sample displaying three regions of different surface activity is shown in figure 5A, which corresponds to bare copper, Cu-BTAH treated for 5 min, and Cu-BTAH treated for 45 min, The BTAH-modified regions were obtained by dipping in the inhibitor-containing solution a freshly-polished copper sample for about a third of its length from either side for the chosen pre-treatment times. In this way, the untreated copper region is to be found in the centre. It is in the central region that the highest current magnitudes are determined as compared to the other two. Conversely, the smallest current magnitude is found above the Cu-BTAH portion pre-treated for 45 min (see figure 5B). Yet, the inhibitive effect of BTAH is already clearly distinguished when the pre-treatment only lasted for 5 min, because the current magnitudes measured from that region are only slightly bigger than those from the region pre-treated for 45 min (cf. figure 2).

It is important to notice that the images shown in figure 5 do not provide any topographical information. The thicknesses of the inhibitor-containing films on copper are below the detection limit. Only changes in the electrochemical activity determined at different locations on the surface of the sample as a result of the different coverage by the inhibitor are visualized. Obviously, the inhibitor covers the surface rather homogeneously for both Cu-BTAH regions since no localized variations in the electrochemical activity are observed within each region.

**Conclusion**

4D AC-SECM has been shown to effectively characterize metal-inhibitor systems from the different current magnitude response obtained at a given frequency for the bare and the covered metal. Differences in local activity of the scanned samples show variations in the frequency dependence of the measured current magnitude, thus allowing to characterize the inhibiting effect of organic molecules and to obtain chemical contrast for 3D imaging with this technique. AC approach curves are sensitive to the electrochemical activity of the sample and to the frequency of the AC excitation signal, thus allowing for extracting information regarding the electrochemical characteristics of the system. Negative feedback type behaviour is observed in the low frequency

range, though it may extend to higher frequency values as the conductive characteristics of the surface are progressively hindered by the growth of the inhibitor film on the otherwise highly conductive metal surface. The high electrochemical contrast provided by AC-SECM even for the investigation of thin inhibitor films such as those obtained from the direct exposure of a copper surface to an inhibitor-containing solution has been demonstrated by scanning the tip over a sample containing regions with the bare metal and other regions with the inhibitor covering the metal, even in the case that differences in the duration of inhibitor adsorption were made. The advantage of AC-SECM is the use of a highly diluted electrolyte without any redox mediator which may influence the corrosion process on the metal surface.

**Experimental section**

Measurements were performed on 99.99% copper purity plates (Goodfellow, UK) of dimensions 3 cm x 3 cm and 1 mm of thickness. The surface of the samples was ground to a 1500 grit finish, followed by two consecutive polishing steps with 1 and 0.3 μm alumina slurries, respectively. The resulting surfaces were degreased with acetone, abundantly rinsed with twice-distilled water and allowed to dry in air.

Benzotriazole (BTAH; Avocado Research Chemicals Ltd., UK, Ref. 15423), 5-methyl-1H-benzotriazole (MBTAH; Aldrich, USA, Ref. 19630-4) were used as received. Potassium chloride (KCl, Riedel de Haën, Seelze, Germany) and sodium sulphate ($Na_2SO_4$, J.T. Baker, Deventer, The Netherlands) were analytical grade quality. Inhibitor solutions were prepared at a 0.1 mM concentration by dissolving the corresponding inhibitor in a 100 mM KCl solution. All aqueous solutions were prepared using ultra-pure water purified with a Milli-Q system from Millipore. Inhibitor films were produced on the copper electrode *ex-situ* by dipping the metallic samples in the inhibitor-containing solution for six different immersion times (5, 10, 15, 30, 45 and 60 min, respectively).

The test electrolyte employed in the 4D AC-SECM measurements was 1 mM $Na_2SO_4$. Platinum microelectrodes were fabricated using 25 μm Pt-wire (Goodfellow, Germany) following a protocol described earlier [49]. A three-electrode configuration was completed with a Pt-wire as counter electrode and an Ag/AgCl pseudo-reference electrode. The copper surface was left unbiased for the duration of the experiments; that is, the samples were at their corresponding open-circuit potential. The 4D AC-SECM set-up and the procedures for SECM imaging in the AC mode have been described somewhere else [39]. AC voltage signals of 100 $mV_{pp}$ amplitude were applied in the 351 to 55493 Hz frequency range. A total of 26 frequency values were used, and the values spaced logarithmically. All AC-SECM scans were made with a tilt correction mode.

**Acknowledgements:**

The authors are grateful to the German Academic Exchange Service (DAAD, Bonn) and to the Spanish Ministry of Science and Innovation (MICINN, Madrid, Acción Integrada No. HA2006-0077) for the grant of a Collaborative Research Programme between Germany and Spain.

**References:**

1. A.C. Bastos, A.M. Simões, S. González, Y. González-García, R.M. Souto, *Electrochem. Commun.* **2004**, 6, 1212.
2. A.C. Bastos, A.M. Simões, M.G. Ferreira, Y. González-García, S. González, R.M. Souto, *Corros. Sci.* **2007**, *49*, 726.
3. A. Simões, D. Battocchi, D. Tallman, G. Bierwagen, *Prog. Org. Coat.* **2008**, *63*, 260.
4. C. H. Paik, H. S. White, R. C. Alkire, *J. Electrochem. Soc*. **2000**, *147*, 4120.
5. C. H. Paik, R. C. Alkire, *J. Electrochem. Soc*. **2001**, *148*, B276.
6. T.E. Lister, P.J. Pinhero, T.L. Trowbridge, R.E. Mizia, *J. Electroanal. Chem.* **2005**, *579*, 291.
7. F. Falkenberg, K. Fushimi, M. Seo, *Corros. Sci*. **2003**, *45*, 2657.
8. C. Gabrielli, S. Joiret, M. Keddam, H. Perrot, N. Portail, P. Rousseau, V. Vivier, *J. Electrochem. Soc*. **2006**, *153*, B68.
9. C. Gabrielli, S. Joiret, M. Keddam, N. Portail, P. Rousseau, V. Vivier, *Electrochim. Acta* **2008**, *53*, 7539.
10. Y.Y. Zhu, D.E. Williams, *J. Electrochem. Soc*. **1997**, *144*, L43.
11. P. James, N. Casillas, W. H. Smyrl, *J. Electrochem. Soc*. **1996**, *143*, 3853.
12. S. B. Basame, H. S. White, *J. Phys. Chem. B* **1998**, *102*, 9812.
13. Y. González-García, G. T. Burstein, S. González, R. M. Souto, *Electrochem. Commun*. **2004**, *6*, 637.
14. L. Freire, X. R. Nóvoa, G. Pena, V. Vivier, *Corros. Sci*. **2008**, *50*, 3205.
15. Y. González-García, S. González, R.M. Souto, *Corros. Sci.* **2005**, *47*, 3312.
16. A.M. Simões, D. Battocchi, D.E. Tallman, G.P. Bierwagen, *Corros. Sci.* **2007**, *49*, 3838.
17. Y. Shao, C. Jia, G. Meng, T. Zhang and F. Wang, *Corros. Sci.* **2009**, *51*, 371.
18. R.M. Souto, L. Fernández-Mérida, S. González, *Electroanalysis* **2009**, *21*, 2640.
19. S.E. Pust, W. Maier, G. Wittstock, *Z. Phys. Chem.* **2008**, *222*, 1463.
20. J. Kwak, A.J. Bard, *Anal. Chem*. **1989**, *61*, 1221.
21. R.D. Martin, P.R. Unwin, *J. Chem. Soc. Faraday Trans*. **1998**, *94*, 753.
22. K. Eckhard, X. Chen, F. Turcu, W. Schuhmann, *Phys. Chem. Chem. Phys*. **2006**, *8*, 5359.
23. V. Radtke, C. Heß, R.M. Souto, J. Heinze, *Z. Phys. Chem.* **2006**, *220*, 393.
24. R.M. Souto, Y. González-García, J. Izquierdo, S. González, *Corros. Sci.* **2010**, *52*, 748.
25. R.M. Souto, Y. González-García, S. González, G.T. Burstein, *Corros. Sci.* **2004**, *46*, 2621.
26. R.M. Souto, Y. González-García, S. González, *Corros. Sci.* **2008**, *50*, 1637.

27. R.M. Souto, Y. González-García, S. González, G.T. Burstein, *Electroanalysis* **2009**, *21*, 2569.
28. K. Mansikkamäki, P. Ahonen, G. Fabricius, L. Murtomäki, K. Kontturi, *J. Electrochem. Soc.* **2005**, *152*, B12.
29. K. Mansikkamäki, C. Johans, K. Kontturi, *J. Electrochem. Soc.* **2006**, *153*, B22.
30. K. Mannsikkamäki, U. Haapanen, C. Johans, K. Kontturi, M. Valden, *J. Electrochem. Soc.* **2006**, *153*, B311.
31. J. Izquierdo, J.J. Santana, S. González, R.M. Souto, *Electrochim. Acta* **2010**, submitted.
32. K. Eckhard, W. Schuhmann, *Analyst* **2008**, *133*, 1486.
33. B. Ballesteros Katemann, A. Schulte, E.J. Calvo, M. Koudelka-Hep, W. Schuhmann, *Electrochem. Commun.* **2002**, *4*, 134.
34. B. Ballesteros Katemann, C. González Inchauspe, P.A. Castro, A. Schulte, E.J. Calvo, W. Schuhmann, *Electrochim. Acta* **2003**, *48*, 1115.
35. A.S. Baranski, P.M. Diakowski, *J. Solid State Electrochem.* **2004**, *8*, 683.
36. C. Gabrielli, F. Huet, M. Keddam, P. Rousseau, V. Vivier, *J. Phys. Chem. B* **2004**, *108*, 11620.
37. P. M. Diakowski, A. S. Baranski, *Electrochim. Acta* **2006**, *52*, 854
38. G. Baril, G. Galicia, C. Deslouis, N. Pebere, B. Tribollet, V. Vivier, *J. Electrochem. Soc*. **2007**, *154*, C108.
39. K. Eckhard, T. Erichsen, M. Stratmann, W. Schuhmann, *Chem. Eur. J.* **2008**, *14*, 3968.
40. K. Eckhard, M. Etienne, A. Schulte, W. Schuhmann, *Electrochem. Commun.* **2007**, *9*, 1793.
41. K. Eckhard, W. Schuhmann, M. Maciejewska, *Electrochim. Acta* **2009**, *54*, 2125.
42. A. Schulte, S. Belger, M. Etienne, W. Schuhmann, *Mater. Sci. Eng. A* **2004**, *378*, 523.
43. D. Ruhlig, W. Schuhmann, *Electroanalysis* **2007**, *19*, 191.
44. M.M. Antonijević, S.M. Milić, M.B. Petrović, *Corros. Sci.* **2009**, *51*, 1228.
45. M.M. Antonijević, S.M. Milić, S.M. Ŝerbula, G.D. Bogdanović, *Electrochim. Acta* **2005**, 50, 3693.
46. Y.N. Prasad, S. Ramanathan, *Electrochim. Acta* **2007**, *52*, 6353.
47. J.H. Chen, Z.C. Lin, S. Chen, L.H. Nie, S.Z. Yao, *Electrochim. Acta* **1998**, *43*, 265.
48. P.M. Diakowski, Z. Ding, *Electrochem. Commun.* **2007**, *9*, 2617.
49. C. Kranz, M. Ludwig, H.E. Gaub, W. Schuhmann, *Adv. Mater.* **1995**, *7*, 568.

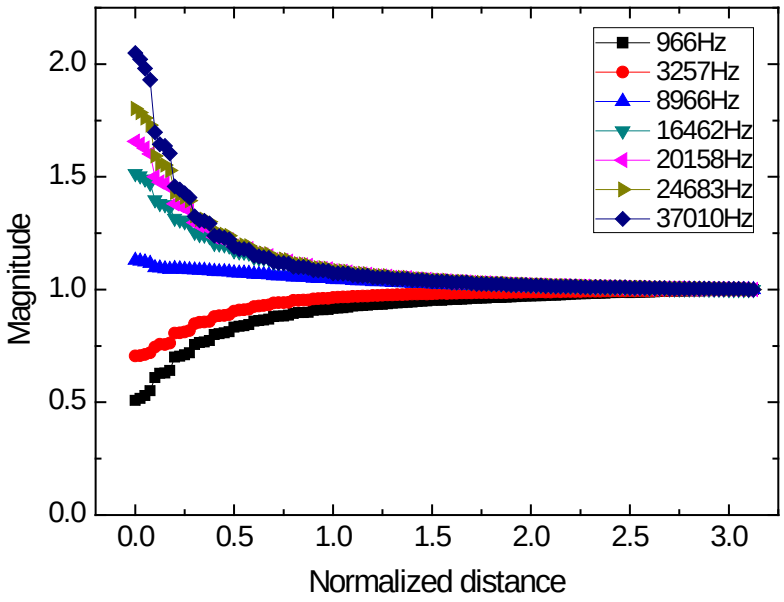


**Figure 1**
Normalized AC approach curves towards a freshly-polished Cu sample immersed in a 10 mM $Na_2SO_4$ solution with a 25 μm electrode. Copper was left at its spontaneous open circuit potential in the electrolyte. The excitation signal amplitude was 100 $mV_{pp}$ and frequencies are indicated in the figure legend.

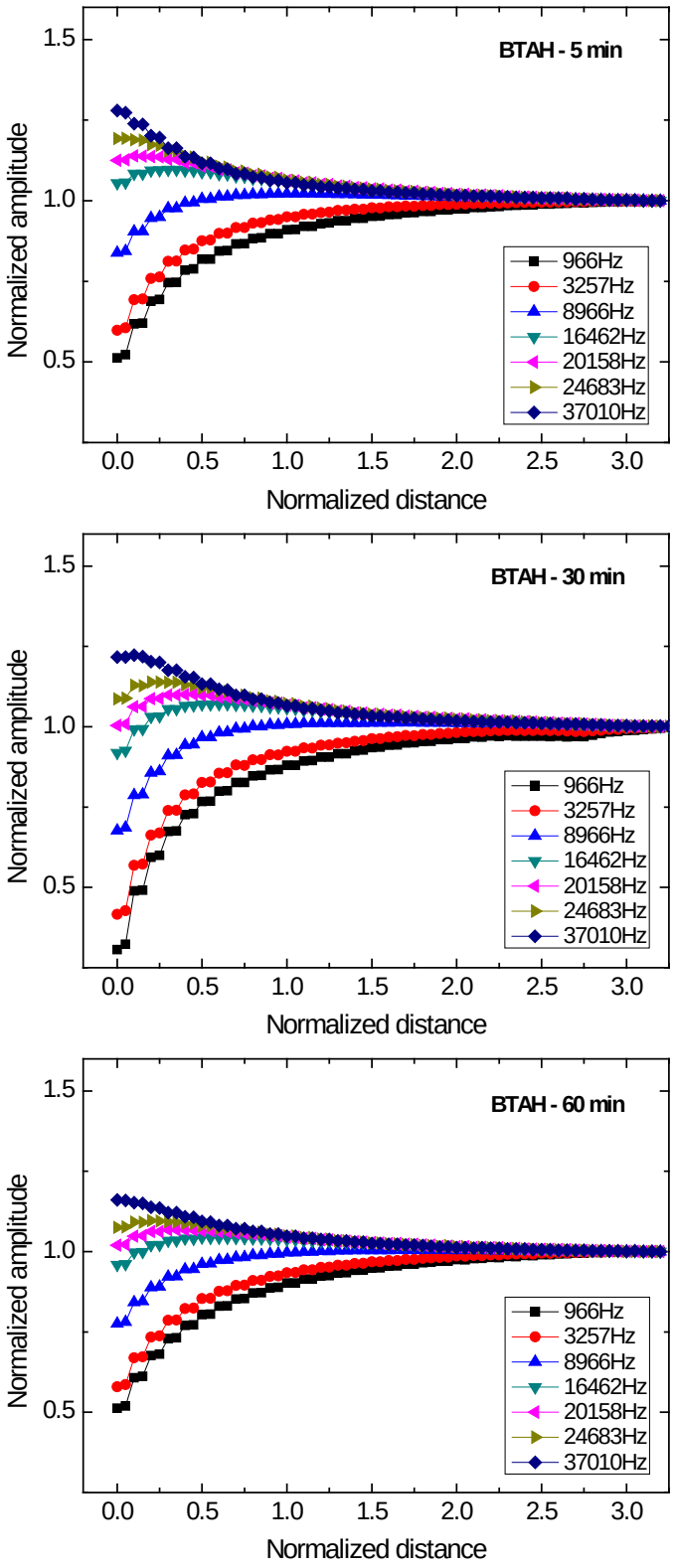


**Figure 2**

Normalized AC approach curves towards BTAH-treated Cu samples immersed in a 10 mM $Na_2SO_4$ solution with a 25 μm electrode. Duration of pre-treatment in the inhibitor containing solution: from bottom to top: 5, 30 and 60 min. The samples were left at their spontaneous open circuit potentials in the electrolyte. The excitation signal amplitude was 100 $mV_{pp}$ and frequencies are indicated in the figure legend.

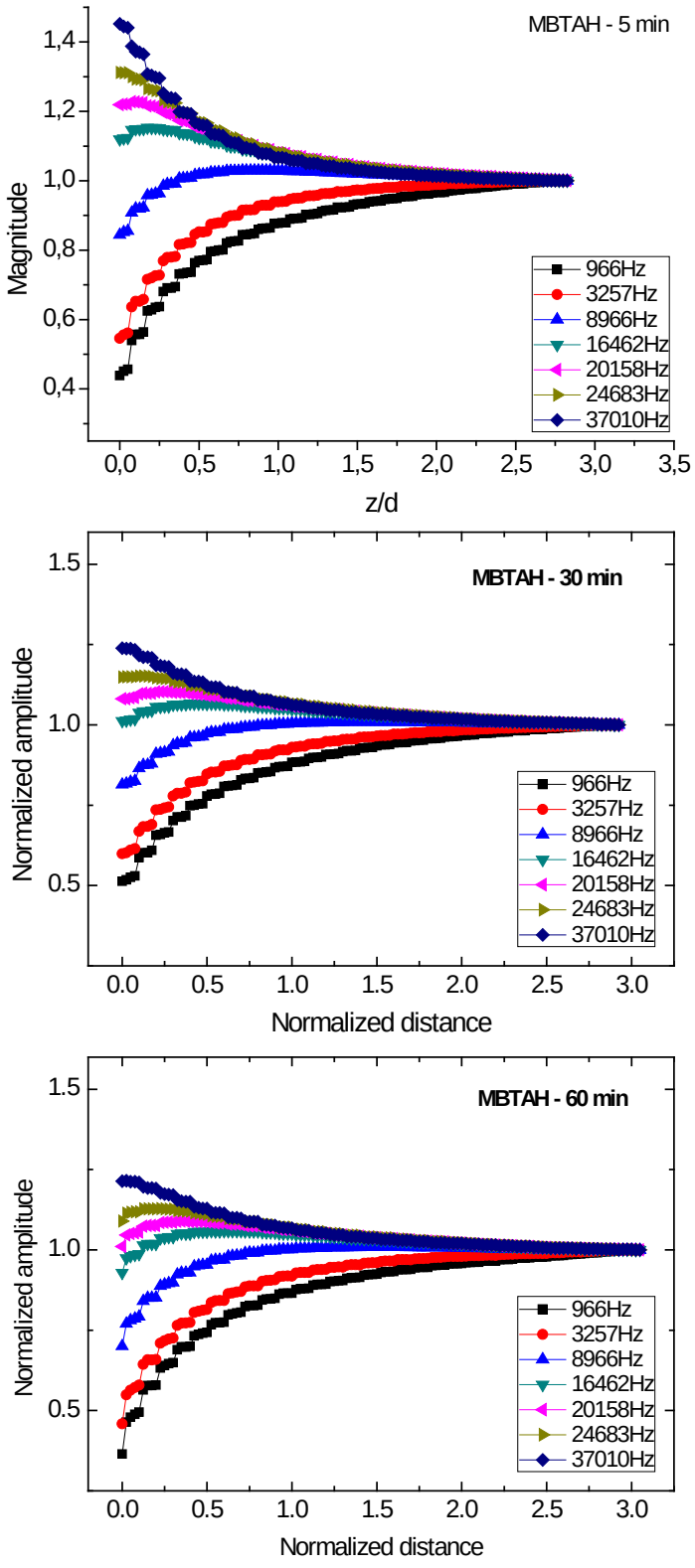


**Figure 3**

Normalized AC approach curves towards MBTAH-treated Cu samples immersed in a 10 mM $Na_2SO_4$ solution with a 25 μm electrode. Duration of pre-treatment in the inhibitor containing solution: from top to bottom: 5, 30 and 60 min. The samples were left at their spontaneous open circuit potentials in the electrolyte. The excitation signal amplitude was 100 $mV_{pp}$ and frequencies are indicated in the figure legend.

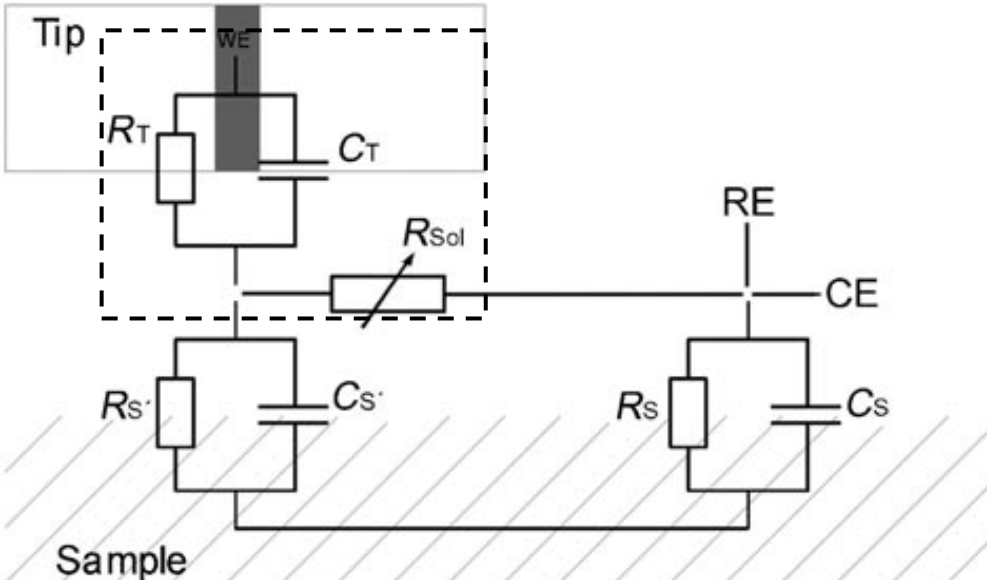


**Figure 4**

Equivalent circuit representing the impedance behaviour of the Cu-inhibitor/electrolyte system. $R_T$ and $C_T$ are resistance and capacitance of the tip, respectively; $R_{sol}$ is the solution resistance; $R_S$ and $C_S$ are the resistance and capacitance of the sample, respectively; $R_{S'}$ and $C_{S'}$ are the local resistance and capacitance of the sample at the specific area covered by the AC-SECM tip.

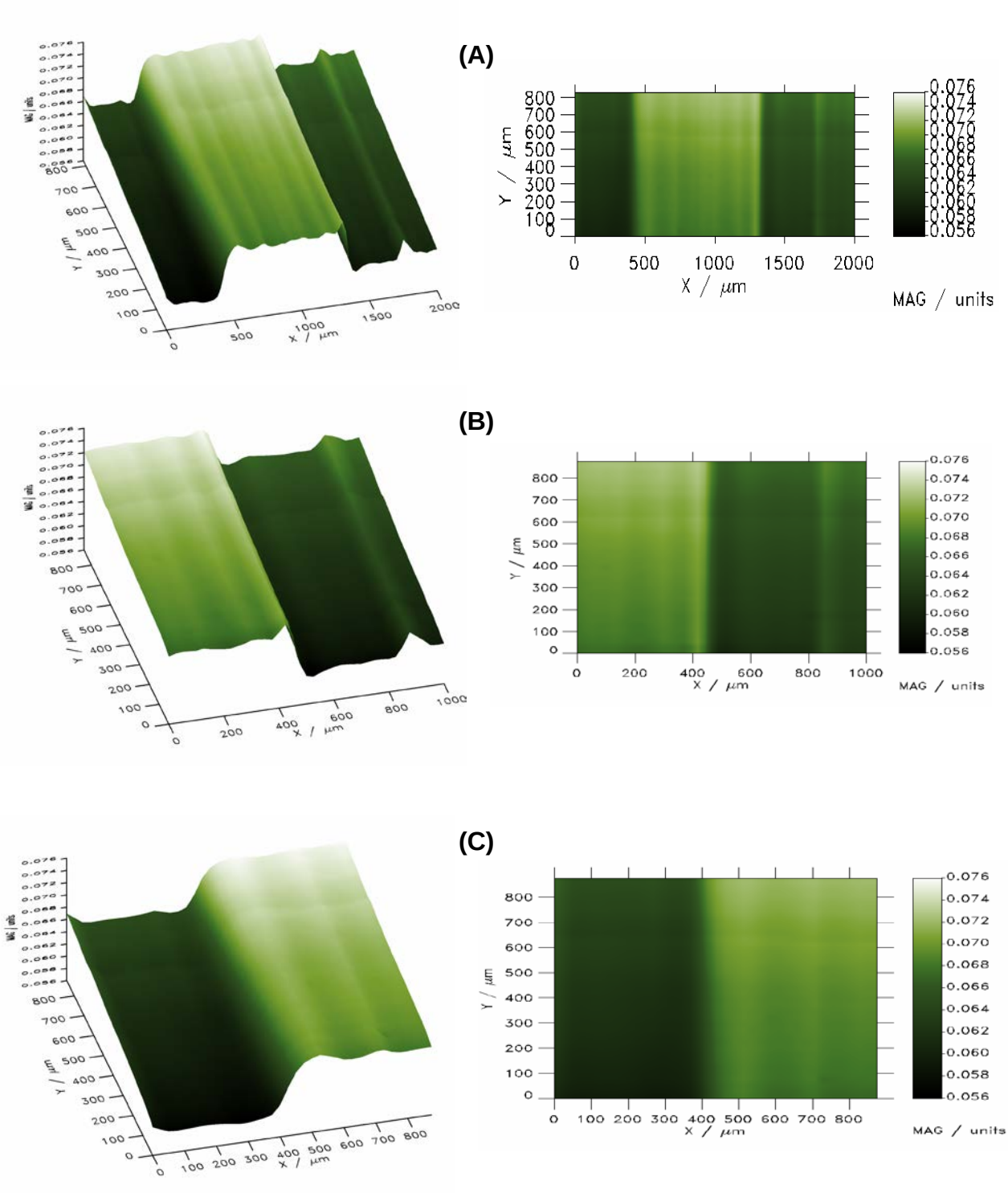


**Figure 5**

AC-SECM measurement on a Cu-BTAH (45 min pre-treatment) – untreated Cu – Cu-BTAH (5 min pre-treatment) system. The different regions on the sample may be found as we move from left to right in the maps. (A) AC-SECM global map depicting the three regions present in the sample; (B) and (C), zooms taken from the global map in (A) for the interphase regions Cu-BTAH (45 min pre-treatment) – untreated Cu and untreated Cu – Cu-BTAH (5 min pre-treatment), respectively. $d$ = 25 μm, $f$ = 8,966 kHz, $c$ = 10 mM $Na_2SO_4$.